IGARSS 2024 - 2024 IEEE International Geoscience and Remote Sensing Symposium | 979-8-3503-6032-5/24/$31.00 ©2024 IEEE | DOI: 10.1109/IGARSS53475.2024.10642040

ANALYSIS OF LAND USE LAND COVER CHANGES AND THEIR IMPACTS ON THE URBAN HEAT ISLAND EFFECT IN BRAGANÇA, PORTUGAL

Cátia Rodrigues de Almeida[1,2,3*], João Alírio[1,2], Artur Gonçalves[3,4], and Ana C. Teodoro [1,2]
[1]Department of Geosciences, Environment and Spatial Planning, University of Porto, Porto, Portugal
[2]Institute of Earth Sciences (ICT), Porto, Portugal
[3]Centro de Investigação de Montanha (CIMO), Instituto Politécnico de Bragança (IPB), Porto, Portugal
[4]Laboratório Associado para a Sustentabilidade e Tecnologia em Regiões de Montanha (SusTEC), Instituto Politécnico de Bragança (IPB), Campus de Santa Apolónia, Porto, Portugal
*up201600831@fc.up.pt

ABSTRACT

The viability of urban life requires a series of changes in Land Use Land Cover (LULC), incorporating anthropic elements at the expense of vegetated areas, changing the land cover, which affects surface albedo. One of the impacts could be the formation of an Urban Heat Island (UHI), where temperatures are higher in cities compared to the vegetated surrounding areas, especially after sunset. Remote Sensing (RS) data, such as Land Surface Temperature (LST), image classification algorithms, and vegetation indices, can be used to understand this dynamic. This research aimed to assess the sensitivity of RS products to LULC changes and evaluate the surface thermal behaviour of (Portugal) between 2016 and 2023, during summer and winter. RS was able to identify some changes in LULC and ascertain that LST, in general, was higher in anthropic areas, especially during the summer.

Index Terms — Land Surface Temperature, Satellite image processing, Google Earth Engine, Land use change, Local Climate Zone

1. INTRODUCTION

To enable housing and basic access for the population in an area, several landscape and Land Use Land Cover (LULC) modifications are necessary. These may include building roads/railways, residences, incorporating irregular and heterogeneous anthropogenic elements, resulting in changes in surface temperature due to alterations in the local albedo (a measure of the rate of reflection of electromagnetic energy by surfaces) [1–7].

When temperatures in urban areas are higher than in the surrounding vegetated areas, we experience the Urban Heat Island (UHI) effect, which can influence the well-being and health of local inhabitants, atmospheric instability, biological risks, etc. [8–14]. Within the UHI, there is a subclassification called Surface Urban Heat Island (SUHI), which corresponds to methodologies that address UHI considering its temporal variability [15].

One of the ways to analyse SUHI and LULC changes includes using Remote Sensing (RS) data, which gathers information about a target without physical interaction with the sensor [14]. In mountainous regions, as proposed in this study, RS can enable data collection that would otherwise be challenging *in situ* [16]. One of the commonly used RS products in SUHI is Land Surface Temperature (LST), which represents the average radiation of the target within the sensor's field of view [17,18]. With the analysis of LST maps, it's possible to identify surface temperatures and, in conjunction with LULC classification methods, pinpoint anthropic areas and verify if they are the warmest. Another method is the computing of the Normalized Difference Vegetation Index (NDVI), which is sensitive to the biomass of a location. Its result varies from -1 to 1, where surfaces with clouds or water show values lower than 0, and areas with healthy vegetation are represented by values close to 1 [19]. There are also products that use a variety of distinct sources, such as RS, topographic surveys, municipal records of zoning and land use, census data, information from urban and environmental planning agencies, and studies conducted by experts and institutions dedicated to urban and environmental planning, which can be used to understand the LULC. The Dynamic World is produced using Google Earth Engine (GEE) and Google AI Plataform, that provides near real-time location-based data, and the Land Use and Occupancy Map (COS), which is official and offers a range of details, can be adapted according to the research objective [20–22].

Considering the availability of RS data and the need to assess the accuracy of these methods, the objective of this study was to determine if surface changes in LULC that occurred between 2016 and 2023 in Bragança - a mountainous region in Portugal - can be identified using RS products, and whether LST is higher in anthropic areas compared to vegetated ones. Bragança was chosen, in fact, because it has been classified into seven different Local Climate Zones (LCZ), based on the consideration of various criteria such as LULC, the height of built structures, and the purpose of their use (residential, industrial, commercial, etc.) [23,24] and features a network of sensors measuring Air Temperature (T_{air}) at 23 different points, allowing us to analyse thermal behaviour based on surface distinctions and respectively compare the thermal behaviour obtained on a satellite scale with local data.

2. STUDY AREA

Located in the extreme northeast of mainland Portugal (41º48`20" N, 6º45`42" W), Bragança is an urban area in a mountainous region with variable altitude, and has around

25,000 inhabitants in an area of approximately 15 km^2. The LULC is heterogeneous, with vegetated areas and open spaces, buildings, commercial and industries [24].

The 23 sensors installed in the city measuring T_{air} are of the TGP-4500 model, TinyTag, Gemini Data Loggers, Chichester, UK. The installation locations followed the classification of the LCZs as follows: i) Compact low-rise (CLR): represented by the old city center, with buildings of medium-low height, high density and the presence of inlaid stone and brick (sensors 4 and 6): ii) Compact midrise (CM): areas with high-density modern construction, medium-high height, and paved surfaces (sensors 3, 7 and 13); iii) Urban green spaces (GAB): urban green spaces, predominantly green, covered with trees and undergrowth (sensors 2, 8, 9 and 11); iv) Large low-rise (LLR): commercial and industrial area, with low or medium density, low and high buildings, with paved parking lots (sensors 5, 17 and 21); v) Open midrise (OM): represented by streets with low or isolated houses of medium density (sensors 10, 12, 18 and 22); vi) Sparsely built (SB): transition space between urban and rural environments, scattered houses with agricultural and forestry surroundings (sensors 1, 14, and 15); and vii) Rural areas (RCD): isolated rural areas on the outskirts of the city (sensors 16, 19, 20 and 23) [24,25] (Figure 1).

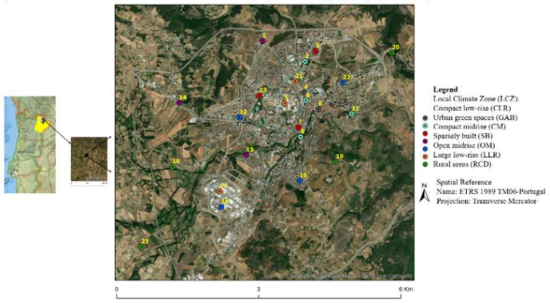

Figure 1. Bragança (Portugal) and the spatial distribution of the 23 sensors used in this study: Compact low-rise (CLR) (gray); Compact midrise (CM) (red); Urban green spaces (GAB) (light green); Large low-rise (LLR) (orange); Open midrise (OM) (blue); Rural areas (RCD) (green); Sparsely built (SB) (purple); (adapted from [25]).

3. DATA ACQUISITION AND PROCESSING

We calculate RS products using the GEE, a cloud-based software that consequently optimizes computer processing/storage time and capacity [25,26]. For image selection, we considered those that had below 20% cloud coverage and additionally applied a cloud mask within the study area to ensure more representative results. The final maps were prepared in ArcGIS Pro. As seasonality influences vegetation behaviour and, consequently, results, we separated some analyses into winter (January, February, and March) and summer (July, August, and September) - periods during which surface thermal behaviour is also influenced by lesser and greater availability of electromagnetic energy due to solar angle, respectively [27,28].

To identify changes in the quantity of vegetated areas, we used Equation 1 [19] and processed the NDVI using the 'COPERNICUS/S2_HARMONIZED' collection from January 11, 2016 to August 26th, 2023, with a spatial resolution of 10 m. We calculated three NDVI maps: i) refers to the average of data obtained in the summer, over the entire period analyzed; ii) the same methodology was applied, but just for the winter period; iii) to identify areas that remain vegetated throughout the analyzed period, we calculate a persistence index. We applied a mask that assigned the value "1" to pixels with NDVI ≥ 0.3 (referring to the presence of vegetation [19]), added these values and divided them by the total number of images, in order to normalize the result between 0 and 1, in each pixel. Finally, to calculate the vegetated areas in each image, we applied a mask considering NDVI values ≥ 0.3 for each pixel and exported these values to a .csv file. To calculate the area, we applied Equation 2.

$$\mathrm{NDVI} = \frac{\mathrm{NIR}-\mathrm{RED}}{\mathrm{NIR}+\mathrm{RED}} \quad (1)\ [19]$$

where NIR is the near-infrared band and RED is the red band.

$$\mathrm{A_{km^2}} = \frac{(\mathrm{N_{pixel}} * \mathrm{A_{pixel}})}{1.000.000} \quad (2)$$

where N_{pixel} is the number of pixels and A_{Pixel} is the pixel resolution, in m^2 (in this case 100 m^2).

We employed a different approach to analyse LULC changes, utilizing the 'GOOGLE/DYNAMICWORLD/V1' collection with a resolution of 10 m. We selected 2016 as the starting year and 2022 as the ending year, considering complete years. The maps were generated using the mode of the class with the highest probability in each pixel. We highlighted distinct classes between the two maps and compared it with the data provided by Google Earth Pro to identify corresponding alterations.

Regarding the LST data, we utilized the data recorded by Landsat 8, specifically from the 'LANDSAT/LC08/C02/T1_L2' collection during the period from March 1st, 2016 to August 12th, 2023, with a spatial resolution of 30 m. We extracted the results for each of the 23 sensors, separated into winter and summer and conducted a correlation using the R software, considering the values obtained in LST and the average values of T_{air} recorded in the *in situ* sensors, between 10 am and 12 pm for compatibility with the Landsat 8 overpass time, which is close to 11 am. Despite not measuring the same physical variables, there some studies compare LST and T_{air} because both are influenced by the availability of electromagnetic energy. In other words, on warmer days, both the surface temperature and the temperature of the lower atmosphere will be higher, and vice versa [25,29–32]. To identify the data distribution, we applied the Shapiro test [33], and since the data did not exhibit normality, we opted for Spearman correlation [34].

Finally, we utilized the COS 2018 dataset to assess the behaviour of LST and determine if temperatures are higher in anthropic areas. We divided the data into summer and winter seasons between 2016 and 2023. We opted to use the same COS dataset due to its updated nature, and since the initial analysis period (2016) is not far removed from this version. We adopted level 2 because anthropic classes are differentiated, while vegetation classes are not disaggregated

[22]. We extracted the average LST value and aggregated it for each distinct class within the COS, level 2. We presented the outcome depicting the average LST within each class during summer and winter.

4. PRELIMINARY RESULTS AND DISCUSSION

For the NDVI data, we processed 141 images, consisting of 100 from summer and 41 from winter. Figure 2 represents the separation of processed images per year. The difference in the number of images can be attributed to cloud cover, resulting in limited data availability for the intended analyses, especially during winter.

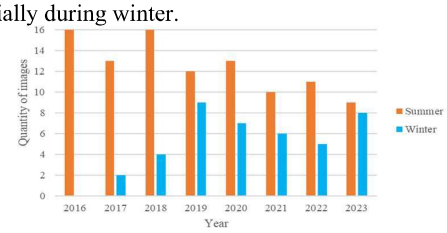

Figure 2. The quantity of images used for the calculation of the Normalized Difference Vegetation Index (NDVI), separated by year and into summer (in orange) and winter (in blue).

Figure 3 shows the average annual area with NDVI ≥ 0.3, divided into summer (orange) and winter (blue). The NDVI exhibited a typical behaviour, with larger areas in summer for most of the years analysed. This can be justified by higher growth activity and vegetation density, contrasting with the more inactive or less dense vegetation conditions during winter [35]. Also, it is worth considering that more images were analysed in summer, which might have interfered with the data variability. In summer, there is a greater and longer incidence of sunlight, alongside higher temperatures, contributing to the seasonal growth of plants and denser foliage due to increased photosynthesis. During winter, many plants shed their leaves and minimize their activities through dormancy [30,36].

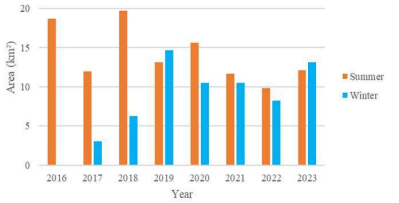

Figure 3. Average annual area with NDVI ≥ 0.3, divided between summer (orange) and winter (blue).

Regarding the average NDVI maps depicted in Figure 4, it is possible to observe the urban area in the center of the map (in shades of yellow) in both the winter and summer maps. Highways and roads are also easily identifiable in both images. In the summer, there are more vegetated areas compared to the winter, which aligns with the results and discussions proposed in the analysis of areas with NDVI ≥ 0.3. It's noteworthy that RS data was able to distinguish seasonality. About the persistent NDVI between 2016 and 2023 (Figure 5), the urban area is characterized as an unchanged area, while the surrounding areas marked in green have changed.

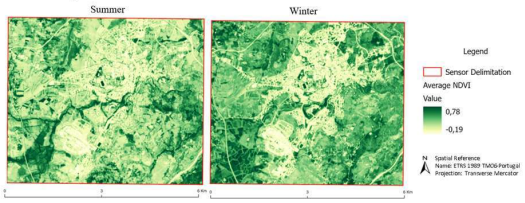

Figure 4. Map of the Normalized Difference Vegetation Index (NDVI) average, for summer and winter (scale ranging from yellow to green, representing -1 and 1, respectively).

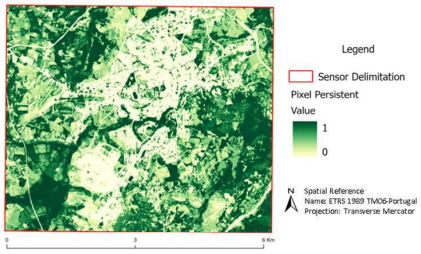

Figure 5. Map of the persistent Normalized Difference Vegetation Index (NDVI) during the analysed period (scale ranging from yellow to green, representing unchanged areas and altered areas, respectively).

Regarding the changes in LULC using 'Dynamic World', seven classes were identified: water, trees, grass, crops, shrub and scrub, built, and bare. When comparing the maps from 2016 to 2023, we noticed changes in the classes, particularly an increase in the built class (red) (Figure 6).

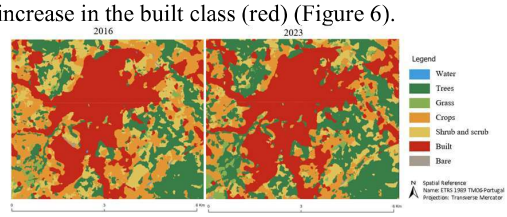

Figure 6. Land Use and Land Cover (LULC) maps for the years 2016 and 2023 (water (blue), trees (dark green), grass (light green), crops (orange), shrub and scrub (yellow), built (red) and bare (brown)).

Figure 7 presents an example of how the method successfully identified a change that occurred during this period in the Tojal de Pereiros street region. About the LST, we processed 45 images, with 33 in the summer and 12 in the winter. The Spearman correlation results between LST and T_{air} (measured with *in situ* sensors) were "strong" and "very strong", considering the scale of $\rho = \pm 0.40$ to ± 0.69 and $\rho \geq \pm 0.70$, respectively [37]. In summer, the average value was $\rho = 0.77$, the minimum was $\rho = 0.64$ (sensor 17), and the maximum was $\rho = 0.91$ (sensor 11). In winter, the average was $\rho = 0.82$, the minimum was $\rho = 0.60$ (sensor 2), and the maximum was

ρ = 0.95 (sensor 22) (Figure 8), providing similar results to a past study conducted in the region [25].

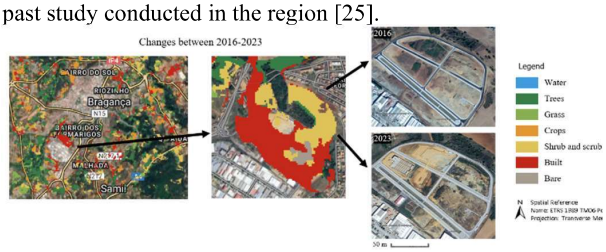

Figure 7. Land Use and Land Cover (LULC) chances between 2016-2023 on Tojal de Pereiros street (water (blue), trees (dark green), grass (light green), crops (orange), shrub and scrub (yellow), built (red) and bare (brown)).

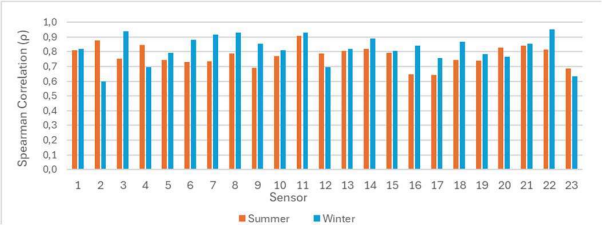

Figure 8. Results of Spearman Correlation between Land Surface Temperature (LST) and Air Temperature (T_{air})

Finally, the average behaviour of LST in the classes of COS 2018 was higher in summer than in winter due to the availability of electromagnetic energy [27,28]. Considering both winter and summer, the four classes that exhibited lower LST values are associated with the presence of vegetation: Brushland, Forests, Permanent crops, and Heterogeneous agricultural areas, supporting studies that link the presence of vegetation as mitigating factors for LST [38] (Table 1).

Table 1. The average behaviour of Land Surface Temperature (LST) within each class of the Land Use and Occupancy Map (COS) 2018.

Class	Summer	Winter
Brushland	34.91	12.99
Built-up areas	42.65	17.22
Equipment	43.01	17.59
Forests	36.52	14.03
Heterogeneous agricultural areas	37.01	13.33
Improved pastures and natural pastures	42.68	18.01
Industry, commerce, and agricultural facilities	38.84	14.48
Inert extraction areas, Waste deposition areas and construction sites	40.82	15.27
Infrastructures	41.75	17.84
Parks and gardens	38.38	15.44
Permanent crops	36.75	13.14
Temporary crops	42.36	16.81
Transportation	41.91	16.23
Average	**39.81**	**15.57**

Regarding the classes with higher values, in summer they were: Equipment, Improved pastures and natural pastures, Built-up areas, and Temporary crops. In winter, three repeated, in order: Improved pastures and natural pastures, Infrastructures, Equipment, and Built-up areas. The presence of the class Improved pastures and natural pastures both in summer and winter can be explained by their configuration: being a horizontal area, there is greater absorption of electromagnetic energy in the early morning hours, coinciding with the satellite's passage around 11 am (Coordinated Universal Time - UTC). These surfaces tend to be warmer compared to those with vertical obstacles (such as urban areas with buildings and areas with trees), due to the projection of shadows [24,25]. Thus, the analysis of SUHI after sunset is advisable, although limited by the availability of RS data. Additionally, the dryness of vegetation in summer can also contribute to heat storage, both for this class and for Temporary crops. Overall, there's a relation between the presence of anthropogenic areas and higher LST values.

In general, there was coherence between the results obtained in the analyzed parameters, as the vegetation areas identified in the LULC show higher NDVI values and the LST values are less intense in LCZs with vegetation presence. In anthropic areas, such as those represented by the urban patch in the center of the study area, the results are inverse, meaning that the NDVI is lower and the LST is more intense.

5. CONCLUSION

Changes in LULC, essential to ensure housing, access, and well-being for the population, can impact the local microclimate due to vegetation suppression and an increase in areas with less permeable materials that have a higher capacity to store electromagnetic energy on their surface.

There are various ways to analyse this impact, as suggested in this research, where we utilized a series of RS products and assessed the methodology's sensitivity in identifying areas with LULC alterations and which classes were associated with higher LST values. Despite Bragança not undergoing significant LULC changes within the analysed period, the RS products managed to highlight some alterations, such as the persistence of vegetation (including seasonality), the construction of roads, and the LST values, which were higher in summer and in anthropic areas.

For future studies, we recommend incorporating other RS data, such as orthophotomaps, drone imagery, and unsupervised classifiers like K-means (which groups pixels into similar clusters) and Principal Component Analysis (PCA) (which reduces data dimensionality while preserving much of the variation, creating a new and independent set of variables). Furthermore, as the initial approach aimed to identify whether RS was a suitable methodology to detect LULC changes, we recommend conducting more detailed analyses of the processed materials to complement the research and contribute to the literature.

ACKNOWLEDGMENTS

The authors are grateful to the Foundation for Science and Technology, I.P., projects UIDB/04683/2020 (https://doi.org/10.54499/UIDB/04683/2020), UIDP/04683/2020 (https://doi.org/10.54499/UIDP/04683/2020, CIMO (UIDB/00690/2020) and SusTEC (LA/P/0007/2020). Cátia Rodrigues de Almeida were financially supported by Portuguese national funds through FCT (Grant: PRT/BD/153518/2021).

7. REFERENCES

1. Oke, T.R. *Boundary Layer Climates*; Routledge, Ed.; 2nd ed.; London, 1987; ISBN 0203407210.
2. Almeida, C.R. de; Teodoro, A.C.; Gonçalves, A. Study of the Urban Heat Island (UHI) Using Remote Sensing Data/Techniques: A Systematic Review. *Environments* **2021**, *8*, 105, doi:10.3390/environments8100105.
3. Min, M.; Lin, C.; Duan, X.; Jin, Z.; Zhang, L. Spatial Distribution and Driving Force Analysis of Urban Heat Island Effect Based on Raster Data: A Case Study of the Nanjing Metropolitan Area, China. *Sustain. Cities Soc.* **2019**, *50*, 101637, doi:10.1016/j.scs.2019.101637.
4. Weng, Q. Fractal Analysis of Satellite-Detected Urban Heat Island Effect. *Photogramm. Eng. Remote Sensing* **2003**, *69*, 555–566, doi:10.14358/PERS.69.5.555.
5. Amanollahi, J.; Tzanis, C.; Ramli, M.F.; Abdullah, A.M. Urban Heat Evolution in a Tropical Area Utilizing Landsat Imagery. *Atmos. Res.* **2016**, *167*, 175–182, doi:10.1016/j.atmosres.2015.07.019.
6. Cui, Y.; Xu, X.; Dong, J.; Qin, Y. Influence of Urbanization Factors on Surface Urban Heat Island Intensity: A Comparison of Countries at Different Developmental Phases. *Sustain.* **2016**, *8*, doi:10.3390/su8080706.
7. Connors, J.P.; Galletti, C.S.; Chow, W.T.L. Landscape Configuration and Urban Heat Island Effects: Assessing the Relationship between Landscape Characteristics and Land Surface Temperature in Phoenix, Arizona. *Landsc. Ecol.* **2013**, *28*, 271–283, doi:10.1007/s10980-012-9833-1.
8. Agam, N.; Kustas, W.P.; Anderson, M.C.; Li, F.; Colaizzi, P.D. Utility of Thermal Image Sharpening for Monitoring Field-Scale Evapotranspiration over Rainfed and Irrigated Agricultural Regions. *Geophys. Res. Lett.* **2008**, *35*, 1–7, doi:10.1029/2007GL032195.
9. Dousset, B.; Gourmelon, F. Satellite Multi-Sensor Data Analysis of Urban Surface Temperatures and Landcover. *ISPRS J. Photogramm. Remote Sens.* **2003**, *58*, 43–54, doi:10.1016/S0924-2716(03)00016-9.
10. Hall, D.K.; Comiso, J.C.; Digirolamo, N.E.; Shuman, C.A.; Key, J.R.; Koenig, L.S. A Satellite-Derived Climate-Quality Data Record of the Clear-Sky Surface Temperature of the Greenland Ice Sheet. *J. Clim.* **2012**, *25*, 4785–4798, doi:10.1175/JCLI-D-11-00365.1.
11. Imhoff, M.L.; Zhang, P.; Wolfe, R.E.; Bounoua, L. Remote Sensing of the Urban Heat Island Effect across Biomes in the Continental USA. *Remote Sens. Environ.* **2010**, *114*, 504–513, doi:10.1016/j.rse.2009.10.008.
12. Mirzaei, M.; Verrelst, J.; Arbabi, M.; Shaklabadi, Z.; Lotfizadeh, M. Urban Heat Island Monitoring and Impacts on Citizen's General Health Status in Isfahan Metropolis: A Remote Sensing and Field Survey Approach. *Remote Sens.* **2020**, *12*, 1–17, doi:10.3390/RS12081350.
13. Oke, T.R. The Energetic Basis of the Urban Heat Island (Symons Memorial Lecture, 20 May 1980). *Q. Journal, R. Meteorol. Soc.* **1982**, *108*, 1–24.
14. Weng, Q.; Lu, D.; Schubring, J. Estimation of Land Surface Temperature-Vegetation Abundance Relationship for Urban Heat Island Studies. *Remote Sens. Environ.* **2004**, *89*, 467–483, doi:10.1016/j.rse.2003.11.005.
15. Weng, Q.; Fu, P. Modeling Annual Parameters of Clear-Sky Land Surface Temperature Variations and Evaluating the Impact of Cloud Cover Using Time Series of Landsat TIR Data. *Remote Sens. Environ.* **2014**, *140*, 267–278, doi:10.1016/j.rse.2013.09.002.
16. Neteler, M. Estimating Daily Land Surface Temperatures in Mountainous Environments by Reconstructed MODIS LST Data. *Remote Sens.* **2010**, *2*, 333–351, doi:10.3390/rs1020333.
17. Hulley, G.C.; Ghent, D.; Göttsche, F.M.; Guillevic, P.C.; Mildrexler, D.J.; Coll, C. *Land Surface Temperature*; 2019; ISBN 9780128144589.
18. Guillevic, P.; Göttsche, F.; Nickeson, J.; Hulley, G.; Ghent, D.; Yu, Y.; Trigo, I.; Hook, S.; Sobrino, J.A.; Remedios, J.; et al. Land Surface Temperature Product Validation Best Practice Protocol Version 1.1. *Best Pract. Satell. L. Prod. Valid. (p. 60) L. Prod. Valid. Subgr.* **2018**, *doi*, 58, doi:10.5067/doc/ceoswgcv/lpv/lst.001.
19. Rouse, J.W.; Haas, R.H.; Schell, J.A.; Deering, D.W. Monitoring Vegetation Systems in the Great Plains with ERTS. *3rd ERTS Symp.* **1973**, 309–317.
20. Dynamic World (Version 2.1) Available online: https://earthengine.google.com/datasets/ (accessed on 20 December 2023).
21. AI Platform.
22. DGTerritório Especificações Técnicas Da Carta de Uso e Ocupação Do Solo (COS) de Portugal Continental Para 2018. **2019**, 60.
23. Stewart, I.D.; Oke, T.R. Local Climate Zones for Urban Temperature Studies. *Bull. Am. Meteorol. Soc.* **2012**, *93*, 1879–1900, doi:10.1175/BAMS-D-11-00019.1.
24. Gonçalves, A.; Ornellas, G.; Ribeiro, A.C.; Maia, F.; Rocha, A.; Feliciano, M. Urban Cold and Heat Island in the City of Bragança (Portugal). *Climate* **2018**, *6*, 1–14, doi:10.3390/cli6030070.
25. Almeida, C.R. de; Furst, L.; Gonçalves, A.; Teodoro, A.C. Remote Sensing Image-Based Analysis of the Urban Heat Island Effect in Bragança, Portugal. *Environ. - MDPI* **2022**, *9*, doi:10.3390/environments9080098.
26. Developers, G. Earth Engine Data Catalog Available online: https://developers.google.com/earth-engine/datasets/catalog/LANDSAT_LC08_C01_T1_SR# description (accessed on 1 August 2021).
27. Almeida, C.; Alírio, J.; Gonçalves, A.; Teodoro, A.C.M. Analysis of the Urban Heat Island in Bragança, Portugal, Using MODIS Data (2003-2022). In Proceedings of the Earth Resources and Environmental Remote Sensing/GIS Applications XIV; Schulz, K., Nikolakopoulos, K.G., Michel, U., Eds.; SPIE: Amsterdã, October 19 2023; p. 15.
28. Zhou, J.; Hu, D.; Weng, Q. Analysis of Surface Radiation Budget during the Summer and Winter in the Metropolitan Area of Beijing, China. *J. Appl. Remote Sens.* **2010**, *4*, 043513, doi:10.1117/1.3374329.
29. Price, J.C. Assessment of the Urban Heat Island Effect Through the Use of Satellite Data. *Mon. Weather Rev.* **1979**, *107*, 1554–1557, doi:10.1175/1520-0493(1979)107<1554:AOTUHI>2.0.CO;2.
30. Rodrigues de Almeida, C.; Garcia, N.; Campos, J.C.; Alírio, J.; Arenas-Castro, S.; Gonçalves, A.; Sillero, N.; Teodoro, A.C. Time-Series Analyses of Land Surface Temperature Changes with Google Earth Engine in a Mountainous Region. *Heliyon* **2023**, *9*, e18846,

doi:10.1016/j.heliyon.2023.e18846.
31. Nichol, J.E.; Fung, W.Y.; Lam, K.; Wong, M.S. Urban Heat Island Diagnosis Using ASTER Satellite Images and 'in Situ' Air Temperature. *Atmos. Res.* **2009**, *94*, 276–284, doi:10.1016/j.atmosres.2009.06.011.
32. Ben-Dor, E.; Saaroni, H. Airborne Video Thermal Radiometry as a Tool for Monitoring Microscale Structures of the Urban Heat Island. *Int. J. Remote Sens.* **1997**, *18*, 3039–3053, doi:10.1080/014311697217198.
33. Shapiro, S.S.; WILK, M.B. An Analysis of Variance Test for Normality (Complete Samples). *Biometrika* **1965**, *52*, 591–611, doi:10.1093/biomet/52.3-4.591.
34. Spearman, C. "General Intelligence," Objectively Determined and Measured. *Am. J. Psychol.* **1904**, *15*, 201, doi:10.2307/1412107.
35. Piao, S.; Fang, J.; Zhou, L.; Guo, Q.; Henderson, M.; Ji, W.; Li, Y.; Tao, S. Interannual Variations of Monthly and Seasonal Normalized Difference Vegetation Index (NDVI) in China from 1982 to 1999. *J. Geophys. Res. Atmos.* **2003**, *108*, doi:10.1029/2002JD002848.
36. Withers, P.C.; Cooper, C.E. Dormancy. In *Encyclopedia of Ecology*; Elsevier, 2008; pp. 952–957.
37. Dancey, C.; Reidy, J. *Statistics Without Maths for Psychology*; 7th ed.; Pearson Education: Harlow, United Kingdom, 2017; ISBN 978-1292128856.
38. Dai, Z.; Guldmann, J.M.; Hu, Y. Thermal Impacts of Greenery, Water, and Impervious Structures in Beijing's Olympic Area: A Spatial Regression Approach. *Ecol. Indic.* **2019**, *97*, 77–88, doi:10.1016/j.ecolind.2018.09.041.